Tropospheric ozone radiative forcing uncertainty due to pre-industrial fire and biogenic emissions

M. J. Rowlinson[1,2], A. Rap[1], D. S. Hamilton[3], R. J. Pope[1,2], S. Hantson[4,5], S. R. Arnold[1], J. O. Kaplan[6], A. Arneth[4], M. P. Chipperfield[1,2], P. M. Forster[7], L. Nieradzik[8]

[1]Institute for Climate and Atmospheric Science, School of Earth and Environment, University of Leeds, Leeds, LS2 9JT, UK.
[2]National Centre for Earth Observation, University of Leeds, Leeds, LS2 9JT, UK.
[3]Department of Earth and Atmospheric Science, Cornell University, Ithaca 14853 NY, USA.
[4]Atmospheric Environmental Research, Institute of Meteorology and Climate research,
Karlsruhe Institute of Technology, 82467 Garmisch-Partenkirchen, Germany.
[5]Geospatial Data Solutions Center, University of California Irvine, California 92697, USA.
[6] Department of Earth Sciences, The University of Hong Kong, Pokfulam Road, Hong Kong.
[7]Priestley International Centre for Climate, University of Leeds, LS2 9JT, Leeds, UK.
[8]Institute for Physical Geography and Ecosystem Sciences, Lund University, Lund S-223 62, Sweden.

Corresponding authors: Matthew J. Rowlinson (ee11mr@leeds.ac.uk); Alex Rap (a.rap@leeds.ac.uk)

1

Abstract Tropospheric ozone concentrations are sensitive to natural emissions of precursor compounds. In contrast to existing assumptions, recent evidence indicates that terrestrial vegetation emissions in the pre-industrial were larger than in the present-day. We use a chemical transport model and a radiative transfer model to show that revised inventories of pre-industrial fire and biogenic emissions lead to an increase in simulated pre-industrial ozone concentrations, decreasing the estimated pre-industrial to present-day tropospheric ozone radiative forcing by up to 34% (0.38 Wm^{-2} to 0.25 Wm^{-2}). We find that this change is sensitive to employing biomass burning and biogenic emissions inventories based on matching vegetation patterns, as co-location of emission sources enhances the effect on ozone formation. Our forcing estimates are at the lower end of existing uncertainty range estimates (0.2 – 0.6 Wm^{-2}), without accounting for other sources of uncertainty. Thus, future work should focus on reassessing the uncertainty range of tropospheric ozone radiative forcing.

Deleted: of

2

1 Introduction

Tropospheric ozone (O_3) is a short-lived greenhouse gas formed in the atmosphere through photochemical oxidation of volatile organic compounds (VOCs) in the presence of nitrogen oxides (NO_x). These precursor gases have both natural and anthropogenic sources, and increased anthropogenic emissions are thought to have caused an increase in global tropospheric O_3 of 25-50% since 1900 (Gauss et al., 2006; Lamarque et al., 2010; Young et al., 2013). The Intergovernmental Panel on Climate Change (IPCC) current best estimate for tropospheric O_3 radiative forcing (RF) over the industrial era is 0.4 ± 0.2 Wm^{-2} with a 5%-95% confidence interval, making tropospheric O_3 the third most important anthropogenic greenhouse gas after CO_2 and CH_4 (Myhre et al., 2013). The present-day (PD) radiative effect (RE) of tropospheric O_3 is relatively well constrained (Rap et al., 2015). The large uncertainty range (0.2-0.6 Wm^{-2}) is caused by a number of factors such as the radiative transfer scheme employed, the model used to simulate tropospheric O_3 and tropopause definition, however it is primarily associated with a poor understanding of pre-industrial (PI) O_3 concentrations (Myhre et al., 2013; Stevenson et al., 2013). Although measurements of tropospheric O_3 exist as far back as the late 19th century, there are limited reliable quantitative measurements of tropospheric O_3 prior to the 1970s (Volz and Kley, 1988; Cooper et al., 2014). Recently Checa-Garcia et al. (2018) found that differences in PI estimates between Coupled Model Intercomparison Project phase 5 (CMIP5) and CMIP6 cause an 8-12% variation in O_3 RF estimates, but did not explicitly assess uncertainty in natural PI emissions. Recent analysis of oxygen isotopes in polar ice cores indicates that tropospheric O_3 in the northern hemisphere increased by less than 40% between 1850 and 2005, suggesting that O_3 RF may be lower than the 0.4 Wm^{-2} estimate (Yeung et al., 2019).

As well as anthropogenic sources, O_3 precursor gases such as methane (CH_4), carbon monoxide (CO) and NO_x have natural emission sources, e.g., wildfires, wetlands, lightning and biogenic emissions. Wildfires, for example, emit large quantities of CO, NO_x, CH_4 and non-methane volatile organic compounds (NMVOCs) (van der Werf et al., 2010; Voulgarakis and Field, 2015), which influence the chemical production of O_3 (Wild, 2007). Changes in the natural environment therefore influence the concentration and distribution of tropospheric O_3 (Monks et al., 2015; Hollaway et al., 2017). While human activities such as deforestation, land-use change and fire management are known to affect natural emission sources of O_3 precursor gases, their impact on emissions net change remains very uncertain (Mickley et al., 2001; Arneth et al., 2010). An accurate representation of PI natural emissions is therefore very important for quantifying the PI to PD tropospheric O_3 RF calculations.

Recent studies suggest that the relationship between humans and fire (Bowman et al., 2009) is more complex than previously assumed (Doerr and Santín, 2016). The expansion of agriculture and land-cover fragmentation since PI has decreased the abundance and continuity of fuel, inhibiting fire spread (Marlon et al., 2008; Swetnam et al., 2016) and hence total emissions. Furthermore, at the global scale, increased population density results in declining fire frequency (Knorr et al., 2014; Andela et al., 2017). Increased agricultural land coupled with active fire suppression and management policies mean that human activity has likely caused total fire emissions to decline since the PI (Daniau et al., 2012; Marlon et al., 2016; Hamilton et al., 2018).

3

Deleted: (Mickley et al., 2001; Arneth et al., 2010). An accurate representation of PI is PI to PD tropospheric O_3 RF calculations.

65   Paleoenvironmental archives of fire activity also reflect a decline of fire over the industrial era in many regions (Marlon et al., 2016; Rubino et al., 2016; Swetnam et al., 2016). This change in understanding of PI fire emissions has been shown to have a strong influence on aerosol RF: Hamilton et al. (2018) estimated a 35-91% decrease in global mean cloud albedo forcing over the industrial era when using revised PI fire emission inventories.

70   Emissions of biogenic VOCs (BVOCs), such as isoprene and monoterpenes, from vegetation also affect tropospheric O_3 formation. Isoprene contributes to the formation of peroxyacetylnitrate (PAN), which has a lifetime of several months in the upper troposphere (Singh, 1987), allowing long-range transport of reactive nitrogen and enhancing O_3 formation in remote regions. PAN formation is also highly dependent on NO_x concentrations, meaning that changes in distribution of emissions as well as the magnitude will impact O_3 formation. Previous studies of PI tropospheric O_3 have often assumed that PI BVOC

75   emissions were equivalent or lower than those in PD (Stevenson et al., 2013). In Stevenson et al. (2013), only one model of the ensemble included PI isoprene emissions that were larger than in the PD simulation. However, BVOC emissions are sensitive to climate, CO_2 concentrations, vegetation type, and foliage density; each of which has changed since the PI (Laothawornkitkul et al., 2009; Hantson et al., 2017) and needs to be accounted for when calculating O_3 RF.

80   The aim of this study is to examine the effect of revised PI fire and BVOC emission inventories on PI to PD tropospheric O_3 RF estimates. We use a global chemical transport model (CTM) and a radiative transfer model to investigate the impact of these revised natural PI emission inventories on tropospheric O_3 PI concentrations and its PI-PD RF. The IPCC 5th assessment report moved to the concept of effective radiative forcing (ERF) (Myhre et al., 2013) to more completely capture the expected global energy budget change from a given driver. However, here we employ the more traditional stratospherically adjusted RF

85   as it can be estimated with more certainty than ERF and previous studies suggest that ERF and RF are likely to be similar for O_3 change (Myhre et al., 2013; Shindell et al., 2013). We note that a number of factors not considered here also introduce uncertainty when simulating PI tropospheric O_3 concentrations, e.g. changes to lightning and soil NO_x emissions, O_3 deposition and atmospheric transport. However, the purpose of this study is to address and focus on the uncertainty associated with natural emissions in the pre-industrial, utilising the revised inventories of fire and biogenic emissions.

90   **2 Methods**

2.1 TOMCAT-GLOMAP

We used the TOMCAT global three-dimensional offline chemical transport model (CTM) (Chipperfield, 2006) coupled to the GLOMAP modal aerosol microphysics scheme (Mann et al., 2010) to simulate tropospheric composition and its response to emissions changes. The model used a 2.8°×2.8° horizontal resolution with 31 vertical levels from the surface to 10 hPa All

95   simulations were run with 6-hourly 2008 meteorology from European Centre for Medium-Range Weather Forecasts (ECMWF) ERA-Interim reanalyses with a 1-year spin-up (Dee et al., 2011). The model includes a detailed representation of hydrocarbon

4

chemistry and isoprene oxidation, and has previously been shown to accurately reproduce observed concentrations and distributions of key tropospheric species such as O_3, CO, NO_x and VOCs (Monks et al., 2017; Rowlinson et al., 2019). The annual global mean surface CH_4 mixing ratio is scaled in TOMCAT-GLOMAP based on observed global mean surface concentrations for the year being simulated; however, the spatial variation in CH_4 concentrations is maintained in the model. Biomass burning and biogenic emissions are emitted into the lowest model level, which extends from the surface to 951 hPa.

2.2 Radiative transfer model

Tropospheric O_3 RFs were calculated using the SOCRATES radiative transfer model (Edwards and Slingo, 1996) with six bands in the shortwave (SW) and nine in the longwave (LW). This version has been used extensively in conjunction with TOMCAT-GLOMAP for calculating O_3 radiative effects (Bekki et al., 2013; Rap et al., 2015; Kapadia et al., 2016; Scott et al., 2018). We used the fixed dynamical heating approximation (Fels et al., 1980) to account for stratospheric temperature adjustments, i.e. changes in stratospheric heating rate calculated in the model due to the O_3 perturbation are applied to the temperature field, with the model run iteratively until stratospheric temperatures reach equilibrium (Forster and Shine, 1997; Rap et al., 2015).

Simulation	Fire emissions	Biogenic emissions
PD CMIP6	GFEDv4	CCMI
PD SIMFIRE-BLAZE	SIMFIRE-BLAZE	CCMI
PI CMIP6	CMIP6	CCMI
PI SIMFIRE-BLAZE	SIMFIRE-BLAZE	CCMI
PI LMfire	LMfire	CCMI
PI CMIP6-BIO	CMIP6	LPJ-GUESS
PI SIMFIRE-BLAZE-BIO	SIMFIRE-BLAZE	LPJ-GUESS
PI LMfire-BIO	LMfire	LPJ-GUESS

Table 1. Details of the TOMCAT-GLOMAP simulations performed in this study.

2.3 Simulations

We investigate the effect of natural PI emissions on PI to PD changes in tropospheric O_3 concentrations, by contrasting PI against PD model simulations (Table 1). All simulations are run with PD meteorology and global mean surface CH_4 concentrations scaled to be 722 ppb in the PI and 1789 ppb in PD (Etheridge et al., 1998; Dlugokencky et al., 2005; Hartmann et al., 2013; McNorton et al., 2016).

5

Deleted: In order to

120   All PI simulations considered anthropogenic emissions set to zero, except for biofuel emissions taken from AeroCom for the year 1750 (Dentener et al., 2006). The first set of three PI simulations (i.e. PI CMIP6, PI SIMFIRE-BLAZE and PI LMfire) investigate the impact of fire emissions only by keeping BVOC emissions (i.e. isoprene and monoterpenes) at their PD values based on the Chemistry-Climate Model Initiative (CCMI) biogenic emissions (Sindelarova et al., 2014). The second set of three PI simulations (i.e. PI CMIP6-BIO, PI SIMFIRE-BLAZE-BIO and PI LMfire-BIO) investigate the additional impact of

125   PI biogenic emissions, by combining each PI fire emission inventory with an estimate of PI BVOC emissions from the LPJ-GUESS model.(Arneth et al., 2007; Schurgers et al., 2009; Smith et al., 2014).

The PD simulations used anthropogenic emissions from the MACCity emissions dataset (from EU projects MACC/CityZEN; Lamarque et al., 2010) and CCMI biogenic emissions (Sindelarova et al., 2014). Two PD simulations were performed, namely

130   the primary PD simulation (PD CMIP) driven by the Global Fire Emissions Database version 4 with small fires (GFED v4s) inventory as employed in CMIP6 (Randerson et al., 2017; van Marle et al., 2017), and PD SIMFIRE-BLAZE (Knorr et al., 2014). A PD simulation is not available for LMfire, a PI fire model not designed to undertake a PD simulation. To isolate the effect of revised natural PI emissions on PI-to-PD tropospheric ozone RF, we compare the 6 PI simulations against the main PD CMIP6 simulation. The other PD simulation, i.e. PD SIMFIRE-BLAZE, is also included in our analysis in order to explore

135   the additional uncertainty in RF introduced by PD emission inventories uncertainties. However, as PD tropospheric ozone RE was shown to be well constrained by satellite observation (Rap et al., 2015), this additional uncertainty is known to be small.

2.4 Fire emission inventories

Following Hamilton et al. (2018), we used three PI inventories to investigate the sensitivity of tropospheric O_3 RF to PI fire

140   uncertainty. The CMIP6 PI inventory is treated as a control, as this has been widely used in previous studies and was developed from a set of global fire models, with SIMFIRE-BLAZE and LMfire providing PI perturbation scenarios from this baseline.

2.4.1 Pre-industrial and present day CMIP6

CMIP6 provides monthly mean emissions of CO, NO_x, CH_4 and VOCs from fires. In the PD, CMIP6 emissions are derived from satellite estimates of global burden area and active fire detections (Randerson et al., 2012; Giglio et al., 2013). In the

145   absence of satellite data, PI CMIP6 fire emissions are generated by merging PD satellite observations with fire proxy records, visibility records and analysis from six fire models (van Marle et al., 2017). The mean of 1750-1770 emissions is used in this study to represent PI emissions. Biomass burning emissions from deforestation and peat fires are assumed to be reduced in the PI, while agricultural fires are kept fairly constant with PD due to a lack of information on the PI environment.

6

2.4.2 Pre-industrial and present day SIMFIRE-BLAZE

150 The SIMFIRE-BLAZE PI fire emission inventory was developed using the LPJ-GUESS-SIMFIRE-BLAZE model. The PI emissions employed here are the mean for the period 1750-1770 (Hamilton et al., 2018). The LPJ-GUESS dynamic vegetation model predicts ecosystem properties for given climate variables (Smith et al., 2014), which, combined with the HYDE 3.1 dataset of human land-use change, allows simulation of global PI land cover (Klein Goldewijk et al., 2011). The SIMple fire model (SIMFIRE) calculates total burned area (Knorr et al., 2014) with total fire carbon-flux calculated from BLAZE (BLAZe

155 induced biosphere-atmosphere flux Estimator) (Rabin et al., 2017). Akagi et al. (2011) emissions factors were used with separate treatment of herbaceous and non-herbaceous, tropical and extratropical vegetation to produce emission inventories. Agricultural fire emissions are not included. Total PI fire emissions of gas species in the SIMFIRE-BLAZE inventory are 28% larger than in the PI CMIP6 inventory.

160 The fire emissions in the PD SIMFIRE-BLAZE model are very similar to the PD CMIP6 inventory, with only slightly increased global NO_x emissions (174 Tg/yr compared to 171 Tg/yr in CMIP6) and CO emissions (1027 Tg/yr compared to 970 Tg/yr). The global distribution of the inventories is also similar (Fig. 1), with slightly larger CO emissions in the SH tropics in PD SIMFIRE-BLAZE, but smaller in the NH tropical region. NO_x and VOC emissions are similar in both inventories across all latitude bands (Fig. 1b, d). The seasonality of emissions is also consistent across both inventories in terms of NO_x and VOC

165 emissions, however for CO the peak in emissions is slightly later for the SIMFIRE-BLAZE inventory (Fig. 3). The slightly higher emissions in PD SIMFIRE-BLAZE result in a simulated tropospheric O_3 burden of 359.9 Tg, an increase of 1% relative to the PD CMIP6 TOMCAT-GLOMAP simulation (Table 2).

2.4.3 Pre-industrial LPJ-LMfire

The LPJ-LMfire model calculates dry matter consumed by fire and simulates natural wildfire ignition from lightning (Pfeiffer

170 et al., 2013; Murray et al., 2014). Land use is prescribed for the year 1770 using the KK10 scenario from Kaplan et al. (2011); climate forcing comes from an 1020-year detrended, interannually variable equilibrium dataset representing late 19th century conditions (see Pfeiffer et al. (2013), sec. 3.4 for details). Akagi et al. (2011) emissions factors were again used to calculate the gas-phase fire emissions from dry biomass burned in each grid cell. Burned area is calculated based on fuel availability. LMfire includes emissions from managed agricultural burning, with 50% of the litter on 20% of used croplands burden

175 annually. Also included are emissions from post-harvest agricultural burning, with 10% of harvested agricultural crop material is assumed to be burned each year. Total PI fire emissions in LMfire are approximately double the SIMFIRE-BLAZE inventory, and thus four times larger than CMIP6 emissions.

7

2.5 Assessment of PI fire emissions

Although the PI LMfire and PI SIMFIRE-BLAZE emissions are substantially larger than the PI CMIP6 emissions, both inventories fall with the current uncertainty range for fire emissions, deemed to differ by up to a factor of ~4 (Lee et al., 2013; Hamilton et al., 2018; Pan et al., 2020). In Hamilton et al. (2018), both the SIMFIRE-BLAZE and LMfire PI inventories were shown to compare more favourably than CMIP6 to changes in PI to PD ice core BC measurements in the Swiss Alps. Furthermore, the LMfire emissions result in simulated aerosol concentrations that were closer to Northern Hemisphere (NH) ice core records in Greenland and Wyoming than both the CMIP6 and SIMFIRE-BLAZE emissions (Hamilton et al., 2018). In addition to the extensive examination of paleoenvironmental archives with PI fire emissions datasets by Hamilton et al. (2018), here we compared simulated annual mean surface PI CO concentrations in Antarctica for each fire emissions inventory using the Southern Hemisphere (SH) ice core CO record from Wang et al. (2010). Simulated Antarctic CO concentrations using PI CMIP6 emissions are 37 ppb, substantially lower than the Wang et al. (2010) 1750 value of 45 ± 5 ppb. This CMIP6 value is closer to the 650-year minimum that occurred in the mid-17th century (38 ppb). When using SIMFIRE-BLAZE and LMfire emissions, Antarctic CO concentrations for 1750 are estimated at 48 ppb and 61 ppb, respectively. The overestimation when using LMfire suggest that SH CO emissions may be high for 1750; however, they are comparable to the peak CO concentration measured in the late 1800s (55 ± 5 ppb) when fire emissions also peaked (van der Werf et al., 2013). As 1850 is also sometimes used as the PI baseline year when calculating RF, we suggest LMfire provides a realistic upper bound to possible PI fire emissions.

The combined evaluation of these inventories in Hamilton et al. (2018) and here indicates that although the revised PI fire inventories differ considerably from each other and are substantially larger than CMIP6 in some regions, they result in simulated PI atmospheric concentrations that more closely represent the changes observed in paleoenvironmental archives of changes in Industrial Era fire activity than CMIP6 estimates do. Therefore, their respective impacts on PI tropospheric O_3 concentrations and RF estimates need to be carefully considered.

2.6 Biogenic emission inventories

2.6.1 Present-day CCMI

The PD control biogenic emissions were provided from the CCMI inventory. CCMI mean annual BVOC emissions, comprising isoprene and monoterpenes, are derived using the Model of Emissions of Gases and Aerosols from Nature (MEGAN) model (Guenther et al., 2012) under the MACC project (Sindelarova et al., 2014). The CCMI inventory estimates global BVOC emissions at 623 Tg/yr, in reasonable agreement with surface flux measurements and other modelling studies (Arneth et al., 2008; Sindelarova et al., 2014; Rap et al., 2018).

2.6.2 Pre-industrial and present day **LPJ-GUESS**

Alternative biogenic emissions were produced using the LPJ-GUESS dynamic vegetation model simulating isoprene and
210 monoterpenes (Arneth et al., 2007; Schurgers et al., 2009). Total PD emissions and distribution in the LPJ-GUESS inventory
(i.e. 607 Tg/yr) are similar to the PD CCMI inventory (Fig. 2). For the PI emissions, the LPJ-GUESS biogenic emissions
inventory is based on the mean for the period 1750-1770, estimated to be 836 Tg/yr. There are large spatial differences between
the PI LPJ-GUESS and PD CCMI inventories, with significantly higher emissions in South America and Central Africa, and
lower emissions in South-East Asia in the PI LPJ-GUESS inventory (Fig. 2).

215 **3 Results and discussion**

3.1 Pre-industrial emission inventories

Figure 1a-d shows annual latitudinal fire emissions of CO, NO_x, CH_4 and VOCs from all sources for the different fire
inventories considered, while Figure 1e compares BVOC emissions (i.e. isoprene and all monoterpenes) from the biogenic
inventories. There is large variation in simulated CO emissions between the three PI fire inventories: 644 Tg/yr in SIMFIRE-
220 BLAZE (69% larger than CMIP6) and 1152 Tg/yr in LMfire (200% larger). Estimates of CO emissions using LMfire results
in total global emissions which are larger than the PD estimate, which also includes anthropogenic sources. The larger PI
biomass burning emissions in LMfire are a result of a number of factors not present in the other PI inventories such as the
inclusion of high-latitude fire occurrence, agricultural fire emissions and differing emission factors (Hamilton et al., 2018).
The largest increase occurs due to increased SH burning in the LMfire inventory, substantially increasing CO emissions from
225 Australia and South America (particularly Eastern Amazonia and Argentina). In the CMIP6 simulations, global CO emissions
are increased by a factor of 2.5 between PI and PD from 382 Tg/yr to 970 Tg/yr. The main driver of this increase is industrial
emissions, particularly in the NH mid-latitudes.

Global NO_x emissions also vary considerably between PI inventories, with values in the SIMFIRE-BLAZE inventory
230 increasing 13% compared to the CMIP6 inventory (36 Tg/yr compared to 32 Tg/yr). This difference is largely due to increased
emission in NH mid-latitudes within SIMFIRE-BLAZE. NO_x emissions in LMfire are 112% larger than the CMIP6 total (68
Tg/yr), with the most significant increases in the extra-tropics.

As CH_4 emissions from fires are significantly smaller than CO emissions (Voulgarakis and Field, 2015), increased PI fire
235 estimates do not substantially alter total CH_4 emission. CH_4 emissions in SIMFIRE-BLAZE and LMfire are similar in amount
and distribution, 15% and 9% lower than CMIP6, respectively. There is an increase in SH CH_4 emissions in both SIMFIRE-
BLAZE and LMfire compared to CMIP6 but a decrease in the NH and SH mid-latitudes. Total PI CH_4 emissions are greatest
in CMIP6 at 241 Tg/yr, approximately 43% of PD emissions. PD SIMFIRE-BLAZE emissions of CH_4 from biomass burning
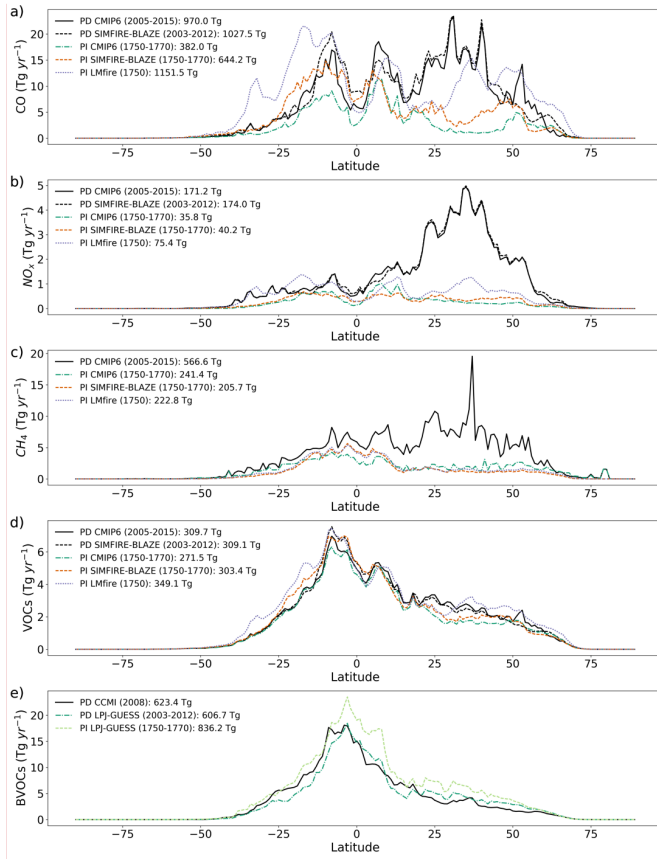
Deleted: ia

240 were not available therefore PD CMIP6 CH_4 was applied in the PD SIMFIRE-BLAZE simulation. Due to the scaling of global mean surface CH_4 concentrations in TOMCAT-GLOMAP, the effect of changes in amount of CH_4 emitted is likely small, however the change in distribution may impact the formation and loss rates of tropospheric O_3.

245 In terms of fire-emitted VOC species, their magnitude and distribution of emissions are fairly consistent between PD and PI inventories. PI CMIP6 are 87% of PD CMIP6 values, with PI SIMFIRE-BLAZE at 97% (303 Tg/yr). Total global VOC emissions are largest in LMfire at 349 Tg/yr, 29% larger than PI CMIP6 (271 Tg/yr) and 13% larger than PD CMIP6 (310 Tg/yr). The distribution of total global VOC emissions is relatively uniform across all inventories; however, individual species do have larger variability between inventories. Formaldehyde and acetylene for example have substantially increased SH
250 emissions in SIMFIRE-BLAZE and LMfire, due to differences in emission factors, vegetation type and burned area between the fire models.
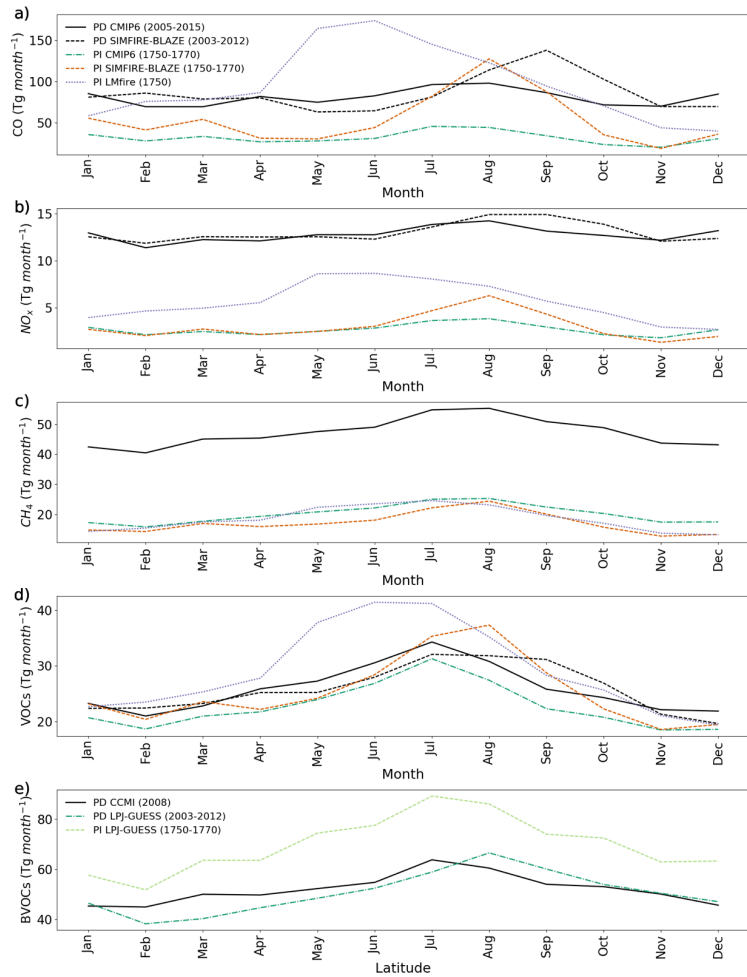
Figure 1: Annual latitudinal mean pre-industrial emissions (in Tg/yr) of (a) CO, (b) NO$_x$, (c) CH$_4$ and (d) VOCs), in PD CMIP6 (solid black line), PD SIMFIRE-BLAZE (dashed black), PI CMIP6 (dashed green), PI SIMFIRE-BLAZE (dotted orange), PI LMfire (dashed purple) inventories,. In (e), annual latitudinal mean BVOC emissions in (Tg/yr) in PD CCMI (solid black line), PD LPJ-GUESS (dashed dark green), PI LPJ-GUESS (dotted light green).

11
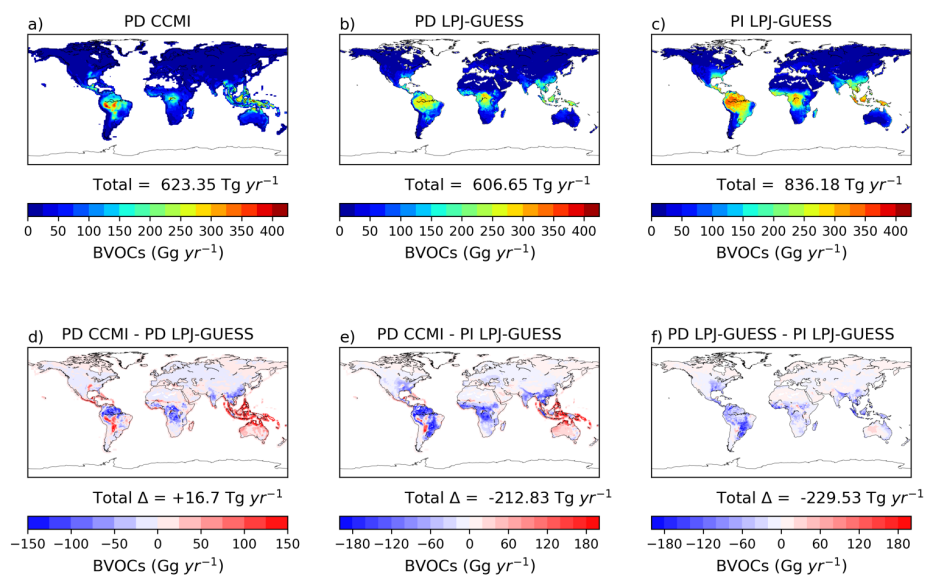
Figure 2: Annual BVOC (isoprene + monoterpenes) emissions at 1°×1° resolution in the two present-day biogenic emissions inventories (CCMI and LPJ-GUESS) and the pre-industrial LPJ-GUESS inventory. Top panels (a-c) show total emissions per year, while lower panels (d-f) show differences between the three inventories. Total annual emissions and difference in annual emissions are also shown.

The BVOC emissions in the two PD inventories (CCMI and LPJ-GUESS) are similar (Fig. 1e), although a small positive NH gradient exists in PD LPG-GUESS compared to PD CCMI. Total BVOC emissions are 16.7 Tg larger in the PD CCMI inventory than PD LPJ-GUESS (Fig. 2). However, the PI LPJ-GUESS BVOC estimate (836 Tg/yr) is 37% larger than its PD equivalent and 34% larger than PD CCMI, although with a similar spatial distribution (Fig. 2). The largest difference is in South American emissions, where PI LPJ-GUESS emissions are up to 120 Tg larger than PD. The reduction of BVOC emissions between PI and PD is due to a combination of crop expansion, land cover changes and CO_2 inhibition (Hantson et al., 2017). Our results are consistent with previous studies reporting between ~25% (Lathière et al., 2010; Pacifico et al., 2012; Hollaway et al., 2017) and ~35% (Unger, 2014) larger PI values than PD.

275 **Figure 3: Total monthly emissions (in Tg/month) of (a) CO, (b) NO$_x$, (c) CH$_4$ and (d) VOCs and total monthly BVOC emissions (e), for PD CMIP6 (solid black line), PD SIMFIRE-BLAZE (dashed black), PI CMIP6 (dashed green), PI SIMFIRE-BLAZE (dotted orange), PI LMfire (dashed purple), PD LPJ-GUESS (dashed dark green) and PI LPJ-GUESS (dotted light green). The legend in panel a) also applies to panels b), c) and d).**

13

280 The seasonality of the fire emissions in the PD and PI inventories used here is demonstrated in Fig. 3. CMIP6 PI and PD emissions have an extremely similar seasonal cycle for all species, with monthly values offset by larger emissions in PD. This is expected as the PI CMIP6 emissions are based on GFED4s climatology and monthly patterns were assumed not to have changed over time (van Marle et al., 2017). The seasonal cycle of CO emissions (Fig. 3a) varies substantially across the 3 PI inventories, with LMfire estimating peak emissions in May-June as opposed to July-August in CMIP6 and SIMFIRE-BLAZE.

285 This may be a result of increased emissions from SH Africa and Central America, where large fire events are common in late spring. The inclusion of high-latitude fire occurrence and agricultural burning in LMfire may also play a role, as these contribute to fire emissions in the boreal spring season (Hamilton et al., 2018). The SIMFIRE-BLAZE CO emissions exhibit a similar but more pronounced seasonal cycle to that in CMIP6, with peak emissions in August. Similarly, NO_x and VOC emissions peak earlier in the year in the LMfire inventory relative to SIMFIRE-BLAZE and CMIP6, again with a larger peak

290 in August in SIMFIRE-BLAZE. Monthly CH_4 emissions are broadly consistent across all inventories, with peak emissions in July or August and lower emissions over the NH winter. The seasonality of BVOCs emissions is also consistent across all PI inventories and PD CMIP6, with a peak in July-August. Isoprene emissions are heavily dependent on temperature and photosynthetic active radiation (Malik et al., 2018), therefore reach a maximum in NH summer when these parameters are optimum for vegetation emissions.

295

Figure 3 indicates similar controls over the modelled seasonality of PI fire occurrence in both PI CMIP6 and PI SIMFIRE-BLAZE, with an increase in estimates fire extent in SIMFIRE-BLAZE results in a more pronounced seasonal cycle. LMfire on the other hand estimates a shift in the seasonality of global fire emissions, with larger fire emissions earlier than other inventories, as well as a broader peak period of emissions. The change in seasonality of precursors will undoubtedly affect the

300 formation and transport of tropospheric O_3, as atmospheric chemistry and circulation also strong have seasonal cycles. However, the broadly similar pattern of maximum emissions in the NH summer and a minimum in winter, coinciding with similar climatic conditions, means that the substantial difference in volume of precursor emissions across the PI inventories is likely to be more significant than seasonal changes.

14
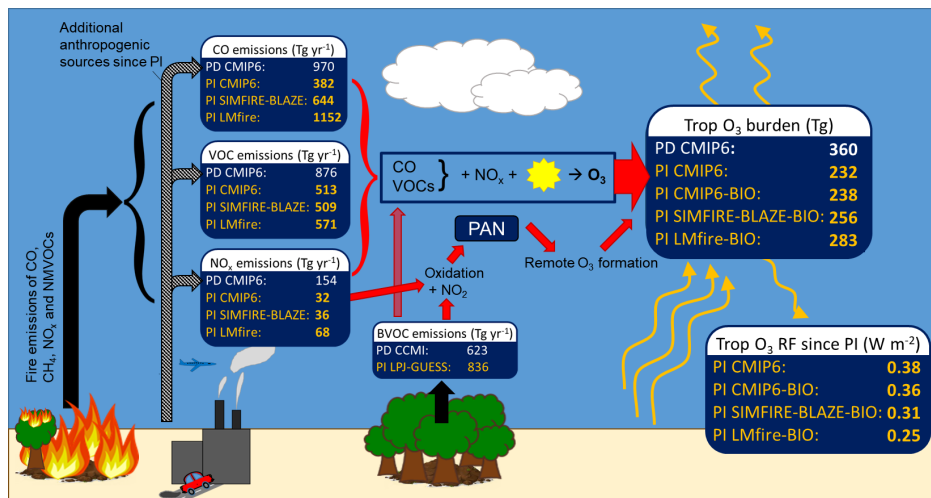
Figure 4: Summary schematic showing tropospheric O₃ precursor emissions from fire, biogenic and anthropogenic sources, the processes of photochemical O₃ formation, the tropospheric O₃ burden and the PI to PD RF. The magnitude of CO, NOₓ, VOC and BVOC precursor emissions used in this study is shown for the PD (white text) and each PI inventory (yellow text). The resulting calculated tropospheric O₃ burden and RF when using each emission inventory are also shown.

3.2 Pre-industrial fire emissions effect on O₃

Annual emissions of O_3 precursors and their contribution to the formation of tropospheric O_3 are shown in Fig. 4. The largest difference between simulations is estimates of the global tropospheric CO burden which varies by up to 100 Tg depending on the PI fire emission inventory employed: 195 Tg in the PI CMIP6 simulation, 232 Tg in PI SIMFIRE-BLAZE (18% higher than CMIP6) and 295 Tg in PI LMfire (50% higher) (Table 2).

The difference in global NO_x burden between PI simulations is less pronounced, with increases of 4% and 18% in PI SIMFIRE-BLAZE and PI LMfire respectively, relative to PI CMIP6. The annual mean NH/SH ratio of tropospheric NO_x burden in PI simulations is 1.09, 1.12 and 1.18 for CMIP6, SIMFIRE-BLAZE and LMfire, respectively. The hydroxyl radical (OH), which plays a key role in regulating tropospheric O_3 concentrations, had lower PI concentrations than in PD due to the higher concentrations of OH precursors NO_x and O_3 in PD outcompeting the effect of increased CH_4 and CO concentrations which deplete OH (Naik et al., 2013). This is consistent in the TOMCAT PI simulations, with airmass-weighted global mean concentrations of tropospheric OH, at 1.06, 1.06 and 1.11 $\times 10^6$ molecules cm^{-3} in CMIP6, SIMFIRE-BLAZE and LMfire, respectively, compared to 1.12 $\times 10^6$ molecules cm^{-3} in PD CMIP6. Each of these values fall within one standard deviation of

15

the Atmospheric Chemistry and Climate Model Intercomparison Project (ACCMIP) multi-model mean of 1.13 ± 0.17 (Naik et al., 2013).

325

Changes to the atmospheric concentration and distribution of O_3 precursor species lead to changes in the tropospheric O_3 burden. The PI CMIP6 simulation produced the lowest tropospheric O_3 burden at 232 Tg, slightly below the ACCMIP multi-model mean of 239 Tg for 1850 (Young et al., 2013). In PI SIMFIRE-BLAZE the burden is 242 Tg (4% higher than CMIP6) while in LMfire it is 273 Tg (18% higher), slightly outside the range of estimates of 1850 tropospheric O_3 burden in ACCMIP

330   models (192 Tg to 272 Tg) (Young et al., 2013). The burdens simulated here represent a PI to PD tropospheric O_3 burden change of 55%, 49% and 32% for CMIP6, SIMFIRE-BLAZE and LMfire, respectively. We note that the PI LMfire emissions is the only inventory leading to a simulated PI to PD global burden change of less than 40%, a value consistent with that recently indicated by isotope measurements in ice cores (Yeung et al., 2019). The differences between CMIP6 and SIMFIRE-BLAZE are primarily related to increases in tropospheric O_3 within the Amazon region (Fig. 5a). The change in tropospheric

335   O_3 vertical profile in the PI SIMFIRE-BLAZE simulation compared to PI CMIP6 (Fig. 5c) shows increased annual mean concentrations throughout the troposphere, driven by changes at 30ºS and 50ºN. Changes between LMfire and CMIP6 simulated tropospheric O_3 profiles are larger, with increased O_3 at all latitudes. Compared to PI CMIP6, there is a mean global increase in O_3 column of 3.7 DU when using LMfire and 1.0 DU when using SIMFIRE-BLAZE. The largest changes occur over Central Asia, Australia and South America where tropospheric column O_3 can be as much as 9.0 DU higher in the PI

340   LMfire simulation than the PI CMIP6 simulation (Fig. 5b). This is reflected in the changes to the vertical O_3 profile, with the largest increases in the subtropics. The difference between LMfire and CMIP6 simulations is greatest between 600 and 800 hPa in the SH and is roughly constant with respect to changes in altitude over the northern subtropics. The only regions where tropospheric O_3 is higher in the CMIP6 simulation are Central Africa and Indonesia, likely due to the PI CMIP6 emissions being anchored to PD fire observations and thus transferring these patterns to the PI (van Marle et al., 2017).

345

The effect of different fire emission inventories on O_3 burden is significantly smaller than the impact on CO concentrations (Table 2), as fire emissions are one of several sources of O_3 variability (Lelieveld and Dentener, 2000). O_3 production is reliant on a number of precursors which do not respond uniformly to the different estimates of fire occurrence in the inventories used here. The relatively minor response of NO_x concentrations across the three PI emissions estimates (Table 2), and the prevailing

350   NO_x-limited state across rural environments in PD (Duncan et al., 2010), suggests that increases in CO and VOCs have only a small impact on O_3 production because of NO_x availability limitations. Moreover, Stevenson et al. (2013) attributed the majority of the PI to PD shift in tropospheric O_3 to NO_x and CH_4 changes, with a relatively small contribution from CO and NMVOCs despite increasing emissions of both. However, the simulated changes still represent significant shifts in the abundance and distribution of tropospheric O_3 in the PI atmosphere.

16

	CO burden (Tg)	NO$_x$ burden (Tg)	Mean tropospheric OH (x10^6 mol cm^{-3})	O$_3$ burden (Tg)	Tropospheric column O$_3$ (DU)	1750-2010 tropospheric O$_3$ RF (Wm^{-2})
PD CMIP6	342.6	73.2	1.12	359.9	31.0	-
PD SIMFIRE-BLAZE	351.6	75.0	1.13	363.5	31.2	-
PI CMIP6	195.5	44.8	1.06	231.7	19.9	0.38
PI SIMFIRE-BLAZE	231.5	46.7	1.06	241.6	20.9	0.35
PI LMfire	295.0	52.8	1.11	272.7	23.6	0.27
PI CMIP6-BIO	238.7	44.3	1.00	237.8	20.2	0.36
PI SIMFIRE-BLAZE-BIO	283.4	46.7	1.00	256.0	22.1	0.31
PI LMfire-BIO	337.1	53.4	1.08	282.8	24.4	0.25

Table 2: Annual mean global tropospheric burdens of CO, NO$_x$ and O$_3$, mean tropospheric OH concentration, tropospheric column O$_3$ for all model simulations and 1750-2010 radiative forc[e] tropospheric O$_3$ estimated for each PI simulation against the PD CMIP6 simulation.
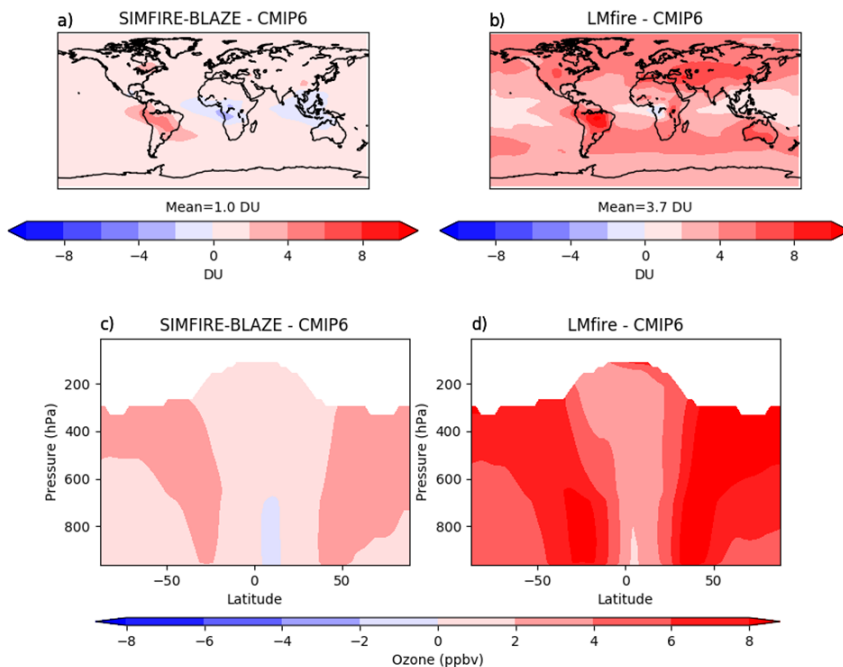
Figure 5: Difference in simulated PI O₃ between revised inventories SIMFIRE-BLAZE and LMfire and the CMIP6 control. Top panels (a, b) compare differences in tropospheric column O₃ in DU, lower panels (c, d) show differences in zonal mean vertical O₃ in ppbv.

3.3 Pre-industrial BVOC emissions effect on O₃

360   We repeated the three PI simulations, replacing the PD biogenic emissions with the PI LPJ-GUESS inventory. In general, the inclusion of PI BVOC emissions increases PI O₃ concentrations, due to an increased VOC source and hence PAN formation (Fig. 4). For CMIP6 fire emissions, the inclusion of PI BVOCs increases the CO burden by 22% and tropospheric O₃ burden by 3%, while mean tropospheric OH concentration decreases by 6%. The decrease in OH is the likely responsible for the simulated increase in CO, as OH is consumed by VOC oxidation. The increase in global tropospheric O₃ indicates that the

365   simulated increases in VOC and CO concentrations are co-located with high NOₓ concentrations, as in low NOₓ BVOCs may decrease local O₃ concentrations. The inclusion of PI BVOCs in the LMfire fire emission simulation causes a 3% decrease in tropospheric OH and increases in tropospheric CO and O₃ of 14% and 4%, respectively.

For SIMFIRE-BLAZE, the inclusion of PI BVOCs decreases OH by 6% and increases CO and O₃ by 22% and 6%, respectively.
370   In all simulations the inclusion of PI BVOCs has only a small effect on the NOₓ burden (~1%). The effect on tropospheric O₃ of including PI BVOCs is notably larger in the simulation using SIMFIRE-BLAZE fire emissions compared to CMIP6 or LMfire. The SIMFIRE-BLAZE simulation combines fire and biogenic emissions produced using the same land-use model, with consistent vegetation distributions. The co-location of isoprene and NOₓ emissions promotes PAN formation, enabling long-range transport of NOₓ and enhancing O₃ production (Hollaway et al., 2017). This synergistic effect has been found to
375   amplify the effect of biogenic emissions on tropospheric O₃ production (Bossioli et al., 2012). Therefore, if PI biogenic

18

emissions inventories were specifically produced for each fire inventory, the corresponding impact on O_3 would likely be larger than presented here. With the inclusion of PI BVOC emissions, both the SIMFIRE-BLAZE and LMfire simulations result in a PI to PD tropospheric O_3 burden change of 40% or less, in line with estimates from oxygen isotope measurements from ice cores (Yeung et al., 2019).

380 **3.4 Effect on ozone radiative forcing**

The estimated tropospheric O_3 RF, based on the CMIP6 PI and PD control simulations, is 0.38 Wm^{-2} (Fig. 4 and Table 2), comparing well with the IPCC AR5 estimate of 0.4 ± 0.2 Wm^{-2} (Myhre et al., 2013; Stevenson et al., 2013). We obtain the same 0.38 Wm^{-2} RF value when contrasting the PI CMIP6 simulation against the other the other PD simulation (PD SIMFIRE-BLAZE). This is consistent with the fact that PD tropospheric O_3 is well constrained by satellite observations (Rap et al., 2015).

385 Given the similarity of the PD simulations, the main PD CMIP6 simulation is used here as the PD for RF calculations in this section. When PI SIMFIRE-BLAZE and PI LMfire emissions are used instead of PI CMIP6 fire emissions, larger PI tropospheric O_3 concentrations lead to 8% (to 0.35 Wm^{-2}) and 29% (to 0.27 Wm^{-2}) decreases in O_3 RF, respectively. When the PI BVOC emission inventory is used in conjunction with each PI fires emission inventory, O_3 RF is further reduced compared to the control by 5% (to 0.36 Wm^{-2}), 18% (to 0.31 Wm^{-2}) and 34% (to 0.25 Wm^{-2}), for CMIP6, SIMFIRE-BLAZE and LMfire,

390 respectively (Fig. 4). While these reductions in O_3 RF are still within the IPCC uncertainty range, they are caused entirely by uncertainty in PI precursor emissions from wildfires and vegetation. Other key sources of uncertainty (e.g. inter-model spread, use of different radiative transfer schemes) are not accounted for here and would therefore alter estimates further, potentially outside the current 5%-95% confidence range. The most important region for changes to the RF of O_3 is the upper troposphere at subtropical latitudes (Fig. 5d), where there are substantially higher O_3 concentrations in the LMfire simulation. O_3 changes

395 in this region are up to 10 times more efficient at altering the radiative flux than in other regions (Rap et al., 2015). However, the lack of a vertical distribution to fire emissions in TOMCAT affects the simulated changes to the O_3 vertical profile. Previous studies which introduced an injection height scheme found small increases in O_3 production downwind of emission sources (Jian and Fu, 2014), although the change to total O_3 and precursors is relatively small (Bossioli et al., 2012; Zhu et al., 2018).

4 Conclusions

400 Revised inventories of PI fire and biogenic emissions substantially decrease estimates of PI to PD tropospheric O_3 RF. When using PI LMfire fire emissions, which represent a plausible upper emissions limit, O_3 RF is reduced to 0.27 Wm^{-2}, 29% smaller than the CMIP6 simulation. Large increases in estimated PI fire occurrence drives increases in PI O_3 concentrations (3.7 DU global mean tropospheric column O_3 increase for LMfire inventory) through larger emissions of CO, NO_x and VOCs. PI CO increases by up to 51% depending on the PI inventory, but the effect on O_3 production is limited by the relatively small increase

405 in NO_x (~4%). Using PI biogenic emissions, rather than assuming PD values, further increases simulated PI tropospheric O_3, though the magnitude of this depends on the fire inventory. When accounting for revised emissions from fire and biogenic sources, both the LMfire and SIMFIRE-BLAZE inventories simulated a PI to PD change in tropospheric O_3 burden of approximately 40% or less, in good agreement with estimates from Yeung et al. (2019). Consequently, we find that the estimate of O_3 RF since PI decreases by up to 34% (to 0.25 Wm^{-2}) when considering the uncertainty in PI emissions of both fires and

410 BVOCs.

The impact on tropospheric O_3 from uncertainty in PI natural emissions suggests that previous estimates of O_3 RF over the industrial era are likely too large. Our revised tropospheric O_3 RF estimates are at the lower end of the existing uncertainty range, without yet taking into account other sources of uncertainty. We therefore argue that the impact of uncertainty in PI

19

415 natural emissions should be further investigated using more models, in order to reassess the current best-estimate and uncertainty range of O_3 RF.

Author contribution

MJR, AR, DSH and RJP conceptualised the study and planned the model experiments. Emission inventories were produced by DH, SH, JOK, AA and LN, and processed for use in TOMCAT-GLOMAP by RJP and DSH. All model runs and analysis was performed by MJR with guidance from AR, RJP and SRA. The manuscript was written by MJR with comments and
430 advice from all co-authors.

20

References

Akagi, S. K., Yokelson, R. J., Wiedinmyer, C., Alvarado, M. J., Reid, J. S., Karl, T., Crounse, J. D., and Wennberg, P. O.:
    Emission factors for open and domestic biomass burning for use in atmospheric models, Atmos. Chem. Phys., 11,
    4039-4072, 10.5194/acp-11-4039-2011, 2011.
Andela, N., Morton, D. C., Giglio, L., Chen, Y., van der Werf, G. R., Kasibhatla, P. S., DeFries, R. S., Collatz, G. J., Hantson,
    S., Kloster, S., Bachelet, D., Forrest, M., Lasslop, G., Li, F., Mangeon, S., Melton, J. R., Yue, C., and Randerson, J.
    T.: A human-driven decline in global burned area, Science, 356, 1356-1362, 10.1126/science.aal4108 %J Science,
    2017.
Arneth, A., Niinemets, Ü., Pressley, S., Bäck, J., Hari, P., Karl, T., Noe, S., Prentice, I. C., Serça, D., Hickler, T., Wolf, A.,
    and Smith, B.: Process-based estimates of terrestrial ecosystem isoprene emissions: incorporating the effects of a
    direct CO_2-isoprene interaction, Atmos. Chem. Phys., 7, 31-53, 10.5194/acp-7-31-2007, 2007.
Arneth, A., Monson, R. K., Schurgers, G., Niinemets, Ü., and Palmer, P. I.: Why are estimates of global terrestrial isoprene
    emissions so similar (and why is this not so for monoterpenes)?, Atmos. Chem. Phys., 8, 4605-4620, 10.5194/acp-8-
    4605-2008, 2008.
Arneth, A., Sitch, S., Bondeau, A., Butterbach-Bahl, K., Foster, P., Gedney, N., de Noblet-Ducoudré, N., Prentice, I. C.,
    Sanderson, M., Thonicke, K., Wania, R., and Zaehle, S.: From biota to chemistry and climate: towards a
    comprehensive description of trace gas exchange between the biosphere and atmosphere, Biogeosciences, 7, 121-149,
    10.5194/bg-7-121-2010, 2010.
Bekki, S., Rap, A., Poulain, V., Dhomse, S., Marchand, M., Lefevre, F., Forster, P. M., Szopa, S., and Chipperfield, M. P.:
    Climate impact of stratospheric ozone recovery, Geophysical Research Letters, 40, 2796-2800, 10.1002/grl.50358,
    2013.
Bossioli, E., Tombrou, M., Karali, A., Dandou, A., Paronis, D., and Sofiev, M.: Ozone production from the interaction of
    wildfire and biogenic emissions: a case study in Russia during spring 2006, Atmos. Chem. Phys., 12, 7931-7953,
    10.5194/acp-12-7931-2012, 2012.
Bowman, D. M. J. S., Balch, J. K., Artaxo, P., Bond, W. J., Carlson, J. M., Cochrane, M. A., D'Antonio, C. M., DeFries, R.
    S., Doyle, J. C., Harrison, S. P., Johnston, F. H., Keeley, J. E., Krawchuk, M. A., Kull, C. A., Marston, J. B., Moritz,
    M. A., Prentice, I. C., Roos, C. I., Scott, A. C., Swetnam, T. W., van der Werf, G. R., and Pyne, S. J.: Fire in the Earth
    System, Science, 324, 481-484, 10.1126/science.1163886, 2009.
Checa-Garcia, R., Hegglin, M. I., Kinnison, D., Plummer, D. A., and Shine, K. P.: Historical Tropospheric and Stratospheric
    Ozone Radiative Forcing Using the CMIP6 Database, Geophysical Research Letters, 45, 3264-3273,
    10.1002/2017GL076770, 2018.
Chipperfield, M. P.: New version of the TOMCAT/SLIMCAT off-line chemical transport model: Intercomparison of
    stratospheric tracer experiments, Quarterly Journal of the Royal Meteorological Society, 132, 1179-1203,
    doi:10.1256/qj.05.51, 2006.
Cooper, O. R., Parrish, D., Ziemke, J., Balashov, N., Cupeiro, M., Galbally, I., Gilge, S., Horowitz, L., R. Jensen, N., Lamarque,
    J.-F., Naik, V., Oltmans, S., Schwab, J., T. Shindell, D., Thompson, A., Thouret, V., Wang, Y., and Zbinden, R.:
    Global distribution and trends of tropospheric ozone: An observation-based review, Elementa: Science of the
    Anthropocene, 2, 000029, 10.12952/journal.elementa.000029, 2014.
Daniau, A. L., Bartlein, P. J., Harrison, S. P., Prentice, I. C., Brewer, S., Friedlingstein, P., Harrison-Prentice, T. I., Inoue, J.,
    Izumi, K., Marlon, J. R., Mooney, S., Power, M. J., Stevenson, J., Tinner, W., Andrič, M., Atanassova, J., Behling,
    H., Black, M., Blarquez, O., Brown, K. J., Carcaillet, C., Colhoun, E. A., Colombaroli, D., Davis, B. A. S., D'Costa,
    D., Dodson, J., Dupont, L., Eshetu, Z., Gavin, D. G., Genries, A., Haberle, S., Hallett, D. J., Hope, G., Horn, S. P.,
    Kassa, T. G., Katamura, F., Kennedy, L. M., Kershaw, P., Krivonogov, S., Long, C., Magri, D., Marinova, E.,
    McKenzie, G. M., Moreno, P. I., Moss, P., Neumann, F. H., Norström, E., Paitre, C., Rius, D., Roberts, N., Robinson,
    G. S., Sasaki, N., Scott, L., Takahara, H., Terwilliger, V., Thevenon, F., Turner, R., Valsecchi, V. G., Vannière, B.,
    Walsh, M., Williams, N., and Zhang, Y.: Predictability of biomass burning in response to climate changes, Global
    Biogeochemical Cycles, 26, GB4007, 10.1029/2011GB004249, 2012.
Dee, D. P., Uppala, S. M., Simmons, A. J., Berrisford, P., Poli, P., Kobayashi, S., Andrae, U., Balmaseda, M. A., Balsamo, G.,
    Bauer, P., Bechtold, P., Beljaars, A. C. M., van de Berg, L., Bidlot, J., Bormann, N., Delsol, C., Dragani, R., Fuentes,
    M., Geer, A. J., Haimberger, L., Healy, S. B., Hersbach, H., Hólm, E. V., Isaksen, L., Kållberg, P., Köhler, M.,
    Matricardi, M., McNally, A. P., Monge-Sanz, B. M., Morcrette, J.-J., Park, B.-K., Peubey, C., de Rosnay, P., Tavolato,
    C., Thépaut, J.-N., and Vitart, F.: The ERA-Interim reanalysis: configuration and performance of the data assimilation
    system, 137, 553-597, 10.1002/qj.828, 2011.
Dentener, F., Kinne, S., Bond, T., Boucher, O., Cofala, J., Generoso, S., Ginoux, P., Gong, S., Hoelzemann, J. J., Ito, A.,
    Marelli, L., Penner, J. E., Putaud, J. P., Textor, C., Schulz, M., van der Werf, G. R., and Wilson, J.: Emissions of
    primary aerosol and precursor gases in the years 2000 and 1750 prescribed data-sets for AeroCom, Atmos. Chem.
    Phys., 6, 4321-4344, 10.5194/acp-6-4321-2006, 2006.
Dlugokencky, E. J., Myers, R. C., Lang, P. M., Masarie, K. A., Crotwell, A. M., Thoning, K. W., Hall, B. D., Elkins, J. W.,
    and Steele, L. P.: Conversion of NOAA atmospheric dry air CH4 mole fractions to a gravimetrically prepared standard
    scale, Journal of Geophysical Research: Atmospheres, 110, doi:10.1029/2005JD006035, 2005.
Doerr, S. H., and Santín, C.: Global trends in wildfire and its impacts: perceptions versus realities in a changing world, 371,
    20150345, doi:10.1098/rstb.2015.0345, 2016.

495   Duncan, B., Yoshida, Y., R. Olson, J., Sillman, S., Martin, R., Lamsal, L., Hu, Y., E. Pickering, K., Retscher, C., and J. Allen, D.: Application of OMI observations to a space-based indicator of NOx and VOC controls on surface ozone formation, Atmospheric Environment, 44, 2213-2223, 10.1016/j.atmosenv.2010.03.010, 2010.

Edwards, J. M., and Slingo, A.: Studies with a flexible new radiation code. I: Choosing a configuration for a large-scale model, Quarterly Journal of the Royal Meteorological Society, 122, 689-719, 10.1002/qj.49712253107, 1996.

500   Etheridge, D. M., Steele, L. P., Francey, R. J., and Langenfelds, R. L.: Atmospheric methane between 1000 A.D. and present: Evidence of anthropogenic emissions and climatic variability, Journal of Geophysical Research: Atmospheres, 103, 15979-15993, doi:10.1029/98JD00923, 1998.

Fels, S. B., Mahlman, J. D., Schwarzkopf, M. D., and Sinclair, R. W.: Stratospheric Sensitivity to Perturbations in Ozone and Carbon Dioxide: Radiative and Dynamical Response, Journal of Atmospheric Sciences, 37, 2265-2297,
505   10.1175/1520-0469(1980)037<2265:Sstpio>2.0.Co;2, 1980.

Forster, P., and Shine, K. P.: Radiative forcing and temperature trends from stratospheric ozone changes, Geophysical Research Letters, 102, 10841-10855, 10.1029/96jd03510, 1997.

Gauss, M., Myhre, G., Isaksen, I. S. A., Grewe, V., Pitari, G., Wild, O., Collins, W. J., Dentener, F. J., Ellingsen, K., Gohar, L. K., Hauglustaine, D. A., Iachetti, D., Lamarque, F., Mancini, E., Mickley, L. J., Prather, M. J., Pyle, J. A.,
510   Sanderson, M. G., Shine, K. P., Stevenson, D. S., Sudo, K., Szopa, S., and Zeng, G.: Radiative forcing since preindustrial times due to ozone change in the troposphere and the lower stratosphere, Atmos. Chem. Phys., 6, 575-599, 10.5194/acp-6-575-2006, 2006.

Giglio, L., Randerson, J. T., and van der Werf, G. R.: Analysis of daily, monthly, and annual burned area using the fourth-generation global fire emissions database (GFED4), 118, 317-328, 10.1002/jgrg.20042, 2013.

515   Guenther, A. B., Jiang, X., Heald, C. L., Sakulyanontvittaya, T., Duhl, T., Emmons, L. K., and Wang, X.: The Model of Emissions of Gases and Aerosols from Nature version 2.1 (MEGAN2.1): an extended and updated framework for modeling biogenic emissions, Geosci. Model Dev., 5, 1471-1492, 10.5194/gmd-5-1471-2012, 2012.

Hamilton, D. S., Hantson, S., Scott, C. E., Kaplan, J. O., Pringle, K. J., Nieradzik, L. P., Rap, A., Folberth, G. A., Spracklen, D. V., and Carslaw, K. S.: Reassessment of pre-industrial fire emissions strongly affects anthropogenic aerosol
520   forcing, Nature Communications, 9, 3182, https://doi.org/10.1038/s41467-018-05592-9, 2018.

Hantson, S., Knorr, W., Schurgers, G., Pugh, T. A. M., and Arneth, A.: Global isoprene and monoterpene emissions under changing climate, vegetation, CO2 and land use, Atmospheric Environment, 155, 35-45, https://doi.org/10.1016/j.atmosenv.2017.02.010, 2017.

Hartmann, D. L., Klein Tank, A. M. G., Rusticucci, M., Alexander, L. V., Brönnimann, S., Charabi, Y., Dentener, F. J.,
525   Dlugokencky, E. J., Easterling, D. R., Kaplan, A., Soden, B. J., Thorne, P. W., Wild, M., and Zhai, P. M.: Observations: Atmosphere and Surface, in: Climate Change 2013: The Physical Science Basis. Contribution of Working Group I to the Fifth Assessment Report of the Intergovernmental Panel on Climate Change, edited by: Stocker, T. F., Qin, D., Plattner, G.-K., Tignor, M., Allen, S. K., Boschung, J., Nauels, A., Xia, Y., Bex, V., and Midgley, P. M., Cambridge University Press, Cambridge, United Kingdom and New York, NY, USA, 159–254, 2013.

530   Hollaway, M. J., Arnold, S. R., Collins, W. J., Folberth, G., and Rap, A.: Sensitivity of midnineteenth century tropospheric ozone to atmospheric chemistry-vegetation interactions, Journal of Geophysical Research, 122, 2452-2473, 10.1002/2016jd025462, 2017.

Jian, Y., and Fu, T. M.: Injection heights of springtime biomass-burning plumes over peninsular Southeast Asia and their impacts on long-range pollutant transport, Atmos. Chem. Phys., 14, 3977-3989, 10.5194/acp-14-3977-2014, 2014.

535   Kapadia, Z. Z., Spracklen, D. V., Arnold, S. R., Borman, D. J., Mann, G. W., Pringle, K. J., Monks, S. A., Reddington, C. L., Benduhn, F., Rap, A., Scott, C. E., Butt, E. W., and Yoshioka, M.: Impacts of aviation fuel sulfur content on climate and human health, Atmos. Chem. Phys., 16, 10521-10541, 10.5194/acp-16-10521-2016, 2016.

Kaplan, J. O., Krumhardt, K. M., Ellis, E. C., Ruddiman, W. F., Lemmen, C., and Goldewijk, K. K.: Holocene carbon emissions as a result of anthropogenic land cover change, The Holocene, 21, 775-791, 10.1177/0959683610386983, 2011.

540   Klein Goldewijk, K., Beusen, A., van Drecht, G., and de Vos, M.: The HYDE 3.1 spatially explicit database of human-induced global land-use change over the past 12,000 years, Global Ecology and Biogeography, 20, 73-86, doi:10.1111/j.1466-8238.2010.00587.x, 2011.

Knorr, W., Kaminski, T., Arneth, A., and Weber, U.: Impact of human population density on fire frequency at the global scale, Biogeosciences, 11, 1085-1102, 10.5194/bg-11-1085-2014, 2014.

545   Lamarque, J. F., Bond, T. C., Eyring, V., Granier, C., Heil, A., Klimont, Z., Lee, D., Liousse, C., Mieville, A., Owen, B., Schultz, M. G., Shindell, D., Smith, S. J., Stehfest, E., Van Aardenne, J., Cooper, O. R., Kainuma, M., Mahowald, N., McConnell, J. R., Naik, V., Riahi, K., and van Vuuren, D. P.: Historical (1850–2000) gridded anthropogenic and biomass burning emissions of reactive gases and aerosols: methodology and application, Atmos. Chem. Phys., 10, 7017-7039, 10.5194/acp-10-7017-2010, 2010.

550   Laothawornkitkul, J., Taylor, J. E., Paul, N. D., and Hewitt, C. N.: Biogenic volatile organic compounds in the Earth system, 183, 27-51, 10.1111/j.1469-8137.2009.02859.x, 2009.

Lathière, J., Hewitt, C. N., and Beerling, D. J.: Sensitivity of isoprene emissions from the terrestrial biosphere to 20th century changes in atmospheric CO2 concentration, climate, and land use, Global Biogeochemical Cycles, 24, 10.1029/2009gb003548, 2010.

555   Lee, L. A., Pringle, K. J., Reddington, C. L., Mann, G. W., Stier, P., Spracklen, D. V., Pierce, J. R., and Carslaw, K. S.: The magnitude and causes of uncertainty in global model simulations of cloud condensation nuclei, Atmos. Chem. Phys., 13, 8879-8914, 10.5194/acp-13-8879-2013, 2013.

22

Lelieveld, J., and Dentener, F. J.: What controls tropospheric ozone?, Journal of Geophysical Research, 105, 3531-3551, 10.1029/1999jd901011, 2000.

560 Malik, T., Gajbhiye, T., and Pandey, S.: Seasonality in emission patterns of isoprene from two dominant tree species of Central India: Implications on terrestrial carbon emission and climate change, 8, 204-212, 2018.

Mann, G., S. Carslaw, K., Spracklen, D., A. Ridley, D., T. Manktelow, P., Chipperfield, M., Pickering, S., and E. Johnson, C.: Description and evaluation of GLOMAP-mode: A modal global aerosol microphysics model for the UKCA composition-climate model, Geosci. Model Dev., 3, 519-551, 10.5194/gmdd-3-651-2010, 2010.

565 Marlon, J. R., Bartlein, P. J., Carcaillet, C., Gavin, D. G., Harrison, S. P., Higuera, P. E., Joos, F., Power, M. J., and Prentice, I. C.: Climate and human influences on global biomass burning over the past two millennia, Nature Geoscience, 1, 697, 10.1038/ngeo313, 2008.

Marlon, J. R., Kelly, R., Daniau, A. L., Vannière, B., Power, M. J., Bartlein, P., Higuera, P., Blarquez, O., Brewer, S., Brücher, T., Feurdean, A., Romera, G. G., Iglesias, V., Maezumi, S. Y., Magi, B., Courtney Mustaphi, C. J., and Zhihai, T.:
570 Reconstructions of biomass burning from sediment-charcoal records to improve data–model comparisons, Biogeosciences, 13, 3225-3244, 10.5194/bg-13-3225-2016, 2016.

McNorton, J., Chipperfield, M., Gloor, M., Wilson, C., Wuhu, F., Hayman, G., Rigby, M., B. Krummel, P., O'Doherty, S., Prinn, R., Weiss, R., Young, D., Dlugokencky, E., and Montzka, S. A.: Role of OH variability in the stalling of the global atmospheric CH4 growth rate from 1999 to 2006, Geophysical Research Letters, 2016, 1-24, 10.5194/acp-
575 2015-1029, 2016.

Mickley, L. J., Jacob, D. J., and Rind, D.: Uncertainty in preindustrial abundance of tropospheric ozone: Implications for radiative forcing calculations, Journal of Geophysical Research, 106, 3389-3399, 10.1029/2000jd900594, 2001.

Monks, P. S., Archibald, A. T., Colette, A., Cooper, O., Coyle, M., Derwent, R., Fowler, D., Granier, C., Law, K. S., Mills, G. E., Stevenson, D. S., Tarasova, O., Thouret, V., von Schneidemesser, E., Sommariva, R., Wild, O., and Williams, M.
580 L.: Tropospheric ozone and its precursors from the urban to the global scale from air quality to short-lived climate forcer, Atmos. Chem. Phys., 15, 8889-8973, 10.5194/acp-15-8889-2015, 2015.

Monks, S., R. Arnold, S., Hollaway, M., Pope, R., Wilson, C., Wuhu, F., Emmerson, K., J. Kerridge, B., Latter, B., M. Miles, G., Siddans, R., and P. Chipperfield, M.: The TOMCAT global chemical transport model v1.6: Description of chemical mechanism and model evaluation, Geosci. Model Dev., 10, 3025-3057, 10.5194/gmd-10-3025-2017, 2017.

585 Murray, L. T., Mickley, L. J., Kaplan, J. O., Sofen, E. D., Pfeiffer, M., and Alexander, B.: Factors controlling variability in the oxidative capacity of the troposphere since the Last Glacial Maximum, Atmos. Chem. Phys., 14, 3589-3622, 10.5194/acp-14-3589-2014, 2014.

Myhre, G., Shindell, D., Bréon, F.-M., Collins, W., Fuglestvedt, J., Huang, J., Koch, D., Lamarque, J.-F., Lee, D., Mendoza, B., Nakajima, T., Robock, A., Stephens, G., Takemura, T., and Zhang, H.: Anthropogenic and Natural Radiative
590 Forcing, in: Climate Change 2013: The Physical Science Basis. Contribution of Working Group I to the Fifth Assessment Report of the Intergovernmental Panel on Climate Change, edited by: Stocker, T. F., Qin, D., Plattner, G.-K., Tignor, M., Allen, S. K., Boschung, J., Nauels, A., Xia, Y., Bex, V., and Midgley, P. M., Cambridge University Press, Cambridge, United Kingdom and New York, NY, USA, 659–740, 2013.

Naik, V., Voulgarakis, A., Fiore, A. M., Horowitz, L. W., Lamarque, J. F., Lin, M., Prather, M. J., Young, P. J., Bergmann,
595 D., Cameron-Smith, P. J., Cionni, I., Collins, W. J., Dalsøren, S. B., Doherty, R., Eyring, V., Faluvegi, G., Folberth, G. A., Josse, B., Lee, Y. H., MacKenzie, I. A., Nagashima, T., van Noije, T. P. C., Plummer, D. A., Righi, M., Rumbold, S. T., Skeie, R., Shindell, D. T., Stevenson, D. S., Strode, S., Sudo, K., Szopa, S., and Zeng, G.: Preindustrial to present-day changes in tropospheric hydroxyl radical and methane lifetime from the Atmospheric Chemistry and Climate Model Intercomparison Project (ACCMIP), Atmos. Chem. Phys., 13, 5277-5298,
600 10.5194/acp-13-5277-2013, 2013.

Pacifico, F., Folberth, G. A., Jones, C. D., Harrison, S. P., and Collins, W. J.: Sensitivity of biogenic isoprene emissions to past, present, and future environmental conditions and implications for atmospheric chemistry, Journal of Geophysical Research, 117, 10.1029/2012jd018276, 2012.

Pan, X., Ichoku, C., Chin, M., Bian, H., Darmenov, A., Colarco, P., Ellison, L., Kucsera, T., da Silva, A., Wang, J., Oda, T.,
605 and Cui, G.: Six global biomass burning emission datasets: intercomparison and application in one global aerosol model, Atmos. Chem. Phys., 20, 969-994, 10.5194/acp-20-969-2020, 2020.

Pfeiffer, M., Spessa, A., and Kaplan, J. O.: A model for global biomass burning in preindustrial time: LPJ-LMfire (v1.0), Geosci. Model Dev., 6, 643-685, 10.5194/gmd-6-643-2013, 2013.

Rabin, S. S., Melton, J. R., Lasslop, G., Bachelet, D., Forrest, M., Hantson, S., Kaplan, J. O., Li, F., Mangeon, S., Ward, D. S.,
610 Yue, C., Arora, V. K., Hickler, T., Kloster, S., Knorr, W., Nieradzik, L., Spessa, A., Folberth, G. A., Sheehan, T., Voulgarakis, A., Kelley, D. I., Prentice, I. C., Sitch, S., Harrison, S., and Arneth, A.: The Fire Modeling Intercomparison Project (FireMIP), phase 1: experimental and analytical protocols with detailed model descriptions, Geosci. Model Dev., 10, 1175-1197, 10.5194/gmd-10-1175-2017, 2017.

Randerson, J. T., Chen, Y., van der Werf, G. R., Rogers, B. M., and Morton, D. C.: Global burned area and biomass burning
615 emissions from small fires, Journal of Geophysical Research, 117, 10.1029/2012jg002128, 2012.

Randerson, J. T., Van Der Werf, G. R., Giglio, L., Collatz, G. J., and Kasibhatla, P. S.: Global Fire Emissions Database, Version 4.1 (GFEDv4), in, ORNL Distributed Active Archive Center, 2017.

Rap, A., Richards, N. A. D., Forster, P. M., Monks, S. A., Arnold, S. R., and Chipperfield, M. P.: Satellite constraint on the tropospheric ozone radiative effect, Geophysical Research Letters, 42, 5074-5081, doi:10.1002/2015GL064037, 2015.

620 Rap, A., Scott, C. E., Reddington, C. L., Mercado, L., Ellis, R. J., Garraway, S., Evans, M. J., Beerling, D. J., MacKenzie, A. R., Hewitt, C. N., and Spracklen, D. V.: Enhanced global primary production by biogenic aerosol via diffuse radiation fertilization, Nature Geoscience, 11, 640-644, 10.1038/s41561-018-0208-3, 2018.

Rowlinson, M. J., Rap, A., Arnold, S. R., Pope, R. J., Chipperfield, M. P., McNorton, J., Forster, P., Gordon, H., Pringle, K. J., Feng, W., Kerridge, B. J., Latter, B. L., and Siddans, R.: Impact of El Niño–Southern Oscillation on the interannual
625 variability of methane and tropospheric ozone, Atmos. Chem. Phys., 19, 8669-8686, https://doi.org/10.5194/acp-19-8669-2019, 2019.

Rubino, M., D'Onofrio, A., Seki, O., and Bendle, J. A.: Ice-core records of biomass burning, The Anthropocene Review, 3, 140-162, 10.1177/2053019615605117, 2016.

Schurgers, G., Arneth, A., Holzinger, R., and Goldstein, A. H.: Process-based modelling of biogenic monoterpene emissions
630 combining production and release from storage, Atmos. Chem. Phys., 9, 3409-3423, 10.5194/acp-9-3409-2009, 2009.

Scott, C. E., Monks, S. A., Spracklen, D. V., Arnold, S. R., Forster, P. M., Rap, A., Äijälä, M., Artaxo, P., Carslaw, K. S., Chipperfield, M. P., Ehn, M., Gilardoni, S., Heikkinen, L., Kulmala, M., Petäjä, T., Reddington, C. L. S., Rizzo, L. V., Swietlicki, E., Vignati, E., and Wilson, C.: Impact on short-lived climate forcers increases projected warming due to deforestation, Nature Communications, 9, 157, 10.1038/s41467-017-02412-4, 2018.

635 Shindell, D. T., Pechony, O., Voulgarakis, A., Faluvegi, G., Nazarenko, L., Lamarque, J. F., Bowman, K., Milly, G., Kovari, B., Ruedy, R., and Schmidt, G. A.: Interactive ozone and methane chemistry in GISS-E2 historical and future climate simulations, Atmos. Chem. Phys., 13, 2653-2689, 10.5194/acp-13-2653-2013, 2013.

Sindelarova, K., Granier, C., Bouarar, I., Guenther, A., Tilmes, S., Stavrakou, T., Müller, J. F., Kuhn, U., Stefani, P., and Knorr, W.: Global data set of biogenic VOC emissions calculated by the MEGAN model over the last 30 years, Atmos.
640 Chem. Phys., 14, 9317-9341, 10.5194/acp-14-9317-2014, 2014.

Singh, H. B.: Reactive nitrogen in the troposphere, Environmental Science & Technology, 21, 320-327, 10.1021/es00158a001, 1987.

Smith, B., Wårlind, D., Arneth, A., Hickler, T., Leadley, P., Siltberg, J., and Zaehle, S.: Implications of incorporating N cycling and N limitations on primary production in an individual-based dynamic vegetation model, Biogeosciences, 11, 2027-
645 2054, 10.5194/bg-11-2027-2014, 2014.

Stevenson, D. S., Young, P. J., Naik, V., Lamarque, J. F., Shindell, D. T., Voulgarakis, A., Skeie, R. B., Dalsoren, S. B., Myhre, G., Berntsen, T. K., Folberth, G. A., Rumbold, S. T., Collins, W. J., MacKenzie, I. A., Doherty, R. M., Zeng, G., van Noije, T. P. C., Strunk, A., Bergmann, D., Cameron-Smith, P., Plummer, D. A., Strode, S. A., Horowitz, L., Lee, Y. H., Szopa, S., Sudo, K., Nagashima, T., Josse, B., Cionni, I., Righi, M., Eyring, V., Conley, A., Bowman, K. W.,
650 Wild, O., and Archibald, A.: Tropospheric ozone changes, radiative forcing and attribution to emissions in the Atmospheric Chemistry and Climate Model Intercomparison Project (ACCMIP), Atmos. Chem. Phys., 13, 3063-3085, 10.5194/acp-13-3063-2013, 2013.

Swetnam, T. W., Farella, J., Roos, C. I., Liebmann, M. J., Falk, D. A., and Allen, C. D.: Multiscale perspectives of fire, climate and humans in western North America and the Jemez Mountains, USA, Philosophical Transactions of the Royal
655 Society B: Biological Sciences, 371, 20150168, doi:10.1098/rstb.2015.0168, 2016.

Unger, N.: Human land-use-driven reduction of forest volatiles cools global climate, Nature Climate Change, 4, 907, 10.1038/nclimate2347, 2014.

van der Werf, G. R., Randerson, J. T., Giglio, L., Collatz, G. J., Mu, M., Kasibhatla, P. S., Morton, D. C., DeFries, R. S., Jin, Y., and van Leeuwen, T. T.: Global fire emissions and the contribution of deforestation, savanna, forest, agricultural,
660 and peat fires (1997–2009), Atmos. Chem. Phys., 10, 11707-11735, 10.5194/acp-10-11707-2010, 2010.

van der Werf, G. R., Peters, W., van Leeuwen, T. T., and Giglio, L.: What could have caused pre-industrial biomass burning emissions to exceed current rates?, Clim. Past, 9, 289-306, 10.5194/cp-9-289-2013, 2013.

van Marle, M. J. E., Kloster, S., Magi, B. I., Marlon, J. R., Daniau, A. L., Field, R. D., Arneth, A., Forrest, M., Hantson, S., Kehrwald, N. M., Knorr, W., Lasslop, G., Li, F., Mangeon, S., Yue, C., Kaiser, J. W., and van der Werf, G. R.:
665 Historic global biomass burning emissions for CMIP6 (BB4CMIP) based on merging satellite observations with proxies and fire models (1750–2015), Geosci. Model Dev., 10, 3329-3357, 10.5194/gmd-10-3329-2017, 2017.

Volz, A., and Kley, D.: Evaluation of the Montsouris series of ozone measurements made in the nineteenth century, Nature, 332, 240-242, https://doi.org/10.1038/332240a0, 1988.

Voulgarakis, A., and Field, R. D.: Fire Influences on Atmospheric Composition, Air Quality and Climate, Current Pollution
670 Reports, 1, 70-81, 10.1007/s40726-015-0007-z, 2015.

Wang, Z., Chappellaz, J., Park, K., and Mak, J. E.: Large Variations in Southern Hemisphere Biomass Burning During the Last 650 Years, Science, 330, 1663-1666, 10.1126/science.1197257, 2010.

Wild, O.: Modelling the global tropospheric ozone budget: exploring the variability in current models, Atmos. Chem. Phys., 7, 2643-2660, 10.5194/acp-7-2643-2007, 2007.

675 Yeung, L. Y., Murray, L. T., Martinerie, P., Witrant, E., Hu, H., Banerjee, A., Orsi, A., and Chappellaz, J.: Isotopic constraint on the twentieth-century increase in tropospheric ozone, Nature, 570, 224-227, 10.1038/s41586-019-1277-1, 2019.

Young, P. J., Archibald, A. T., Bowman, K. W., Lamarque, J. F., Naik, V., Stevenson, D. S., Tilmes, S., Voulgarakis, A., Wild, O., Bergmann, D., Cameron-Smith, P., Cionni, I., Collins, W. J., Dalsøren, S. B., Doherty, R. M., Eyring, V., Faluvegi, G., Horowitz, L. W., Josse, B., Lee, Y. H., MacKenzie, I. A., Nagashima, T., Plummer, D. A., Righi, M., Rumbold,
680 S. T., Skeie, R. B., Shindell, D. T., Strode, S. A., Sudo, K., Szopa, S., and Zeng, G.: Pre-industrial to end 21st century projections of tropospheric ozone from the Atmospheric Chemistry and Climate Model Intercomparison Project (ACCMIP), Atmos. Chem. Phys., 13, 2063-2090, 10.5194/acp-13-2063-2013, 2013.

Zhu, L., Val Martin, M., Gatti, L. V., Kahn, R., Hecobian, A., and Fischer, E. V.: Development and implementation of a new biomass burning emissions injection height scheme (BBEIH v1.0) for the GEOS-Chem model (v9-01-01), Geosci. Model Dev., 11, 4103-4116, 10.5194/gmd-11-4103-2018, 2018.

685